New magnetic resonance imaging methods in nephrology

Jeff L. Zhang, PhD,
Radiology, University of Utah

Glen Morrell, MD, PhD,
Radiology, University of Utah

Henry Rusinek, PhD,
Radiology, New York University

Eric Sigmund, PhD,
Radiology, New York University

Hersh Chandarana, MD, PhD,
Radiology, New York University

Lilach O. Lerman, MD, PhD,
Nephrology & Hypertension, Mayo Clinic, Rochester, MN

Pottumarthi Vara Prasad, PhD,
Radiology, North Shore University

David Niles, MSc,
Medical Physics, University of Wisconsin-Madison

Nathan Artz, PhD,
Medical Physics, University of Wisconsin-Madison

Sean Fain, PhD,
Medical Physics, University of Wisconsin-Madison

Pierre H. Vivier, MD,
Radiology, Rouen University Hospital, France

Alfred K. Cheung, MD, and
Division of Nephrology and Hypertension, University of Utah

Vivian S. Lee, MD, PhD
Radiology, University of Utah

Abstract

Correspondence: Jeff L. Zhang, 729 Arapeen Drive, Department of Radiology, Salt Lake City, UT, 84108, Tel: 801 587 8112, Lei.Zhang@hsc.utah.edu.

Established as a method to study anatomic changes, such as renal tumors or atherosclerotic vascular disease, magnetic resonance imaging (MRI) to interrogate renal function has only recently begun to come of age. In this review, we briefly introduce some of the most important MRI techniques for renal functional imaging, and then review current findings on their use for diagnosis and monitoring of major kidney diseases. Specific applications include renovascular disease, diabetic nephropathy, renal transplants, renal masses, acute kidney injury and pediatric anomalies. With this review, we hope to encourage more collaboration between nephrologists and radiologists to accelerate the development and application of modern MRI tools in nephrology clinics.

Keywords

kidney; magnetic resonance imaging; glomerular filtration rate; tissue oxygenation; perfusion

INTRODUCTION

Long established as a method to study structural changes in disease, such as renal tumors or atherosclerotic vascular disease, magnetic resonance imaging (MRI) to interrogate renal function has only recently begun to come of age. Functional renal MR approaches render added value for MRI over other conventional imaging modalities, with emerging applications in nephrology. As an example, low doses of the conventional contrast agent used in MRI – gadolinium chelates – can be used to measure glomerular filtration rate in individual kidneys [1, 2]. Techniques borrowed from functional brain mapping known as Blood Oxygen Level Dependent (BOLD) MRI have recently been applied to interrogate renal oxygenation and metabolic rate [3, 4]. Renal perfusion can be measured using MRI either by intravenous injection of an exogenous tracer or with endogenous blood labeling methods that do not require contrast injection.

In this article, we briefly review the principles of MR imaging, introduce some of the most important MRI techniques, and then review current findings on their use for diagnosis and monitoring of major kidney diseases. Specific applications include renovascular disease, diabetic nephropathy, renal transplants, renal masses, acute kidney injury and pediatric anomalies. Our purpose is to accelerate the application of modern MRI tools in the clinic and to strengthen the collaboration between MRI physicists, radiologists and nephrologists. We refer the reader to other reviews [5–14] and the cited papers for more technical details.

MRI PRINCIPLES AND TECHNIQUES

Modern clinical MRI scanners are typically equipped with a large superconducting magnet, which provides a stable homogeneous magnetic field (1.5 – 3.0 Tesla), and multiple coils for different purposes, including signal transmission, reception and creating magnetic field gradients. For abdominal imaging, surface coils are available to be applied to the abdomen to improve signal reception. Due to the strong magnetic field, pacemakers are usually contraindicated with MRI scans, but most vascular stents are compatible.

Most MRI signals originate from hydrogen nuclei or protons, which behave like tiny magnets in the MRI system's magnetic field and their behavior in response to changing magnetic fields forms the basis of MRI. MRI image contrast is achieved by manipulating the magnetic properties of hydrogen protons and thereby distinguishing among various tissue characteristics, including intrinsic MR properties like the relaxation times T_1 and T_2. Compared to tissues, water (e.g. cysts, cerebrospinal fluid) typically has longer T_1 and T_2 times (Figure 1).

Using MRI we can also visually distinguish tissues based on other inherent tissue properties such as diffusivity of water within those tissues, capillary perfusion, blood flow or velocity, and even oxygenation. Additionally, with the administration of exogenous contrast agents, other tissue characteristics can be explored. Exogenous agents like gadolinium (Gd) based chelates are useful for MR angiography and in MR renography because they shorten T_1 relaxation time, and for many years were regarded as one of the safest agents used in medicine. About a decade ago, the associations between high doses (typically double and triple the standard doses) of Gd contrast in patients with renal failure and nephrogenic systemic fibrosis (NSF) were first reported [15]. Recommendations have been made on the use of Gd contrast in patients with renal impairment [16, 17]. In the last few years with adherence to guidelines, no report of new NSF cases has been published [18].

Below we review some of the MRI techniques most widely explored for applicability to functional renal imaging. Their characteristics are summarized in Table 1.

MR Renography (MRR) and Dynamic Contrast-Enhanced (DCE) MRI

MR renography (MRR) is a term used to describe one application of dynamic contrast-enhanced (DCE) MRI, specifically, the use of Gd-based contrast agents for the noninvasive measurement of glomerular filtration rate (GFR). Most Gd chelates have favorable renal properties: freely filtered at the glomeruli without tubular secretion or resorption. This means that with the continuous acquisition of high resolution images through the kidney every few seconds, renal function can be visualized as the passage of contrast material from the aorta through the kidney and out of the collecting system. Calculation of the extraction fraction of the Gd contrast allows determination of GFR. Several technical limitations have slowed the widespread adoption of this method, although recent developments are promising. We review some of the challenges below.

Unlike CT or nuclear medicine, where tracer concentration is approximately linear to signal intensity, in DCE MRI, the relationship is more complex and it depends on the specific pulse sequence used. Methods converting MR signal intensity to concentrations of tracer have been reviewed elsewhere [19, 20]. Because of the sensitivity of MRI to Gd contrast agents, 3–4 ml of Gd contrast agent suffices for accurate renal functional measurements. In MRR, signal intensities can be recorded from the whole kidney to determine GFR. For more refined measurements, signal intensities can be recorded from the renal cortex, medulla and collecting system. With more detailed data, the transit of the bolus of contrast from the artery to the renal cortex can be used to estimate renal perfusion; the transit from cortex to medulla reflects glomerular filtration; and finally from the medulla into the collecting system reflects tubular function.

To extract these functional measurements from signal intensities in the kidney, the method typically assumes a tight bolus of contrast entering the renal artery. Gd contrast is administered intravenously, and therefore accurate measurement of renal function depends on knowing the shape of the bolus of contrast as it arrives in the abdominal aorta, following dispersion during transit through the pulmonary circulation, heart, and thoracic aorta. Direct measurement of the bolus as it arrives at the level of the renal arteries can be measured from images of the abdominal aorta and is termed as arterial input function (AIF). Using a mathematical operation called deconvolution we can eliminate the variable effects of bolus dispersion, as quantified by AIF, on the measurements of tracer in the kidney. Compartmental modeling is typically used to extract renal physiological parameters like GFR from enhancement curves. The details of the models and their comparison can be found in literature [2, 21–25].

Several studies have shown good agreement between MRR measurements of GFR and reference methods. Hackstein et al [26] found a correlation coefficient of 0.83 between MRR-GFR and GFR measured by iopromide plasma clearance. Using low Gd dose (4 ml) and multiple-compartment modeling technique, Lee et al [2, 21, 24] measured MRR-GFR with correlation coefficient of 0.82–0.84 with ^{99m}Tc-DTPA plasma clearance.

One major issue with MRR is imprecise measurement of arterial input function (AIF). Cutajar et al [27] found that AIF errors could severely lower the precision of the estimated GFR and renal blood flow. Zhang et al [28] proposed a technique of using patient's cardiac output (measured using phase-contrast MRI) and increased the correlation coefficient between two independent MRR-GFR measurements from 0.83 to 0.92. The cardiac-output approach [28] is promising in correcting for AIF errors, but measurement of the patient's cardiac output with phase-contrast MRI can be cumbersome [29]. The other parameters such as vascular and tubular mean transit times (MTT) measure the time it takes for unfiltered and filtered tracers to go through a kidney, respectively. While clinically able to distinguish different renal pathologies [30], the accuracy of these parameters has not been validated.

Another hurdle to the clinical use of MRR is the absence of dedicated processing software on commercial workstations. For pediatric applications, several programs are freely downloadable on the web [31, 32]. Additionally, for analysis of adult data, recent software developments appear promising in their simplicity of use and potential widespread dissemination [33, 34].

Blood oxygen level dependent (BOLD)

Renal BOLD MRI is a method similar to functional imaging in the brain [35] that forms images of a particular tissue characteristic, the transverse relaxation time constant T_2^*. T_2^* is strongly affected by deoxyhemoglobin, whose paramagnetic effect shortens T_2^*. This gives a potential window into the oxygen level throughout the kidney. Some investigators prefer the use of R_2^* (=$1/T_2^*$). Higher R_2^* (or low T_2^*) theoretically corresponds to higher deoxyhemoglobin, and in turn, lower tissue pO_2 level.

Several groups have demonstrated the sensitivity of BOLD imaging to different physiologic states in both human and animal kidneys. Hypoxia in the renal medulla of rat and pig

models, measured with oxygen probes, has been shown to improve after administration of the loop diuretic furosemide [36, 37]. Corresponding increases in medullary T_2* (increase in oxygenation) with furosemide administration or with water diuresis have been reported in animal models [37, 38] and normal humans [3]. Some studies have shown that the changes in T_2* after furosemide administration or water diuresis are attenuated in diabetic kidneys [39, 40] and in elderly subjects [41]. Some other studies have shown that the basal T_2* values (without diuretic challenge) negatively correlate with the degree of diabetic nephropathy (eGFR level in humans [42], and days after induction of diabetes in a rat model [43]).

Given the central role of hypoxia in the progression of chronic kidney disease [44–46], the prospect of assessing renal parenchymal oxygenation level by non-invasive techniques is exciting. However, published renal BOLD data appear to be somewhat contradictory, with some studies failing to show these aforementioned effects [47, 48]. The contradictions may be partly due to the technical challenges of BOLD MRI. One such challenge is the low signal-to-noise ratio (SNR) of conventional renal BOLD images. The kidneys move during respiration, and this excursion limits BOLD imaging to a single breath hold. A short imaging time results in the low SNR and consequently decreases in the precision of T_2* estimation. To overcome this problem, we have recently developed a new BOLD imaging technique during free breathing [49] which allows longer imaging times, thus improving the T_2* precision significantly (Figure 2). Another factor that may have caused the contradiction in the publications is the multiple confounding factors other than tissue pO_2 that influence T_2* [50, 51], such as blood perfusion, intrinsic transverse relaxation not due to deoxyhemoglobin, volume fraction of blood in a voxel and magnetic field strength (1.5T vs 3T). To quantify absolute tissue oxygenation based on BOLD T_2*, it is necessary to measure the above confounding factors in vivo and address their effects. In addition, the BOLD signal, which is primarily due to the microscopic susceptibility effect of deoxyhemoglobin, could sometimes be superimposed by signals from macroscopic susceptibility artifact. Magnetic field shimming to improve the magnetic field homogeneity [52] can help reduce the impact of such artifact.

Arterial spin labeling (ASL)

Originally used in the brain for perfusion and functional imaging, arterial spin labeling (ASL) MR imaging [53, 54] uses arterial blood as an endogenous contrast agent, and obviates any exogenous agent as in DCE MRI. In this approach, the MR system is used to regionally label inflowing arterial blood by altering its magnetic state. The labeled blood then transits to the tissue where its magnetization affects the measured signal intensity, and the degree of signal change reflects tissue perfusion.

Typically, ASL requires two types of images: *label* and *control*. The two images are acquired in exactly the same way, except that before acquiring the *label* image, magnetization of some arterial blood is altered or labeled. Subtraction of the *control* from the *label* images provides a *difference* image, and the *difference* is solely due to the labeled magnetization of arterial blood in the part of the body being imaged. Examples of *difference* image are shown in Figure 3 [55, 56]. To estimate renal perfusion, the labeling is typically done at abdominal aorta, and the labeled blood transits through renal vascular space, like an

exogenous tracer. Unlike an exogenous tracer, the altered magnetization of labeled blood recovers toward its baseline pre-labeled state within a few seconds due to T_1 relaxation. This means that the transit time for the labeled arterial blood to move into the perfused organ should be short enough to maintain measurable *difference* signals.

Due to concerns about nephrogenic systemic fibrosis (NSF) [57–59], non-contrast imaging techniques such as ASL are particularly attractive for patients with advanced renal diseases as well as allograft dysfunction, where it can be used for longitudinal perfusion evaluation (see 'Renal Transplants' section). One technical challenge with kidney ASL is the respiratory motion associated with long scan time (minutes) for achieving sufficient SNR. These errors can be mitigated, however, using a variety of approaches including: synchronized breathing, respiratory triggering, or retrospective sorting based on respiratory position [60–62]. For example, Gardener and Francis [63] proposed a rapid multi-slice ASL technique for the kidneys and used retrospective image sorting to correct for the respiratory motion artifact.

Recent studies have tested ASL in native and transplanted kidneys with both normal and altered function [55, 60–62, 64–81]. Two main ASL methods have been used: FAIR ASL and pseudocontinuous ASL (pCASL), details of which can be found elsewhere [82, 83]. Renal perfusion measured using a FAIR ASL scheme, first demonstrated in the kidneys by Martirosian et al. [55], has correlated with renal artery stenosis grades [69], renal plasma flow [69, 76], and microsphere perfusion measurements [65]. Artz et al. [64] found that FAIR-ASL yielded reproducible cortical perfusion results in native and transplanted kidneys, although the reproducibility for medulla was moderate to poor. ASL has detected significantly lower perfusion in allografts vs. healthy kidneys [60], native diseased vs. healthy kidneys [74, 78], and in renal allografts experiencing an acute decrease in renal function (>20% increase in serum creatinine) compared to allografts with good function (serum creatinine < 2mg/dl) [73]. A background-suppressed, pseudocontinuous ASL (pCASL) method [61] has helped characterize renal masses [75] and enabled distinction between histopathological diagnoses such as oncocytomas and renal cell carcinomas [72]. Finally, ASL measurements have correlated with clinical outcome in patients with metastatic renal cell carcinoma undergoing antiangiogenic therapy [67].

Overall, while early clinical ASL results appear promising for differentiating different disease states, validation and development of robust quantitative perfusion methods remain under investigation.

Diffusion weighted MRI (DWI)

Diffusion-weighted MR imaging probes micron-scale water motion in tissue [84]. During the imaging period, relative displacement of water molecules due to diffusion in the presence of magnetic field gradients results in a decay in the DWI signals. Such decay can be quantified by the "apparent diffusion coefficient" (ADC), which is computed as the decay constant of the exponential signal decay. ADC is influenced by microstructural barriers. In the case of anisotropic diffusion in ordered structures such as renal medulla, diffusion tensor imaging (DTI) [85–87] can be applied to measure both the magnitude and the 3D direction of diffusion (Figure 4). DTI requires more data using multiple gradient directions. In another variant of

DWI with MR parameters designed to be highly sensitized to perfusion, referred to as intravoxel incoherent motion (IVIM) imaging [88], both tissue diffusion and perfusion-like characteristics can be extracted from DWI images.

DWI has recently found increasing application extracranially including characterization of kidney function [89–91]. Progress to date indicates promising sensitivity of DWI to renal function [70, 92], but further experiments and analysis are needed to disentangle the relevant biophysical mechanisms and yield further diagnostic specificity.

APPLICATIONS FOR KIDNEY DISEASES

Renovascular Diseases

Renal MR angiography has long been established as an accurate, clinically-acceptable method for depicting renal artery stenosis [93–95]. Because of the high incidence of asymptomatic renal artery stenosis, several methods have been investigated as adjuncts to anatomic imaging to help determine the functional significance of the stenosis, to monitor therapy, and to develop predictive indices to identify patients likely to benefit from revascularization.

To assess the functional significance of the renovascular disease (RVD), renal blood flow (RBF) can be measured using ASL or DCE MRI, using as Gd contrast agents or ultra-small paramagnetic ironoxide (USPIO) particles that stay in the intravascular space. Using USPIO-enhanced imaging, Schoenberg et al found that with renal artery diameter narrowing less than 80%, intrarenal cortical perfusion did not change significantly (average 513 ml/100 g/min), while artery narrowing more than 80% caused a fall of more than 200 ml/100 g/min in cortical perfusion[96, 97]. ASL-MRI uses spin-labeled arterial blood as the tracer, thereby avoiding the potential adverse effects of exogenous contrast agents. Its value in RVD remains to be determined.

The management of RVD, often asymmetric in nature, may benefit from the determination of single-kidney GFR using MRR. The detection of hemodynamically significant renal artery stenosis (RAS), often corresponding to >70% decrease in diameter, can be facilitated by the administration of angiotensin converting enzyme inhibitors (ACEI). ACEI attenuates GFR and thus the magnitude of signal enhancement in the presence of significant renal artery stenosis [98], but this attenuation is difficult to determine in subjects with low basal signal enhancement. To overcome this barrier, a multi-compartmental modeling method for analyzing dual-injection MRI data has been developed to allow for GFR determinations in human kidneys with significant stenotic renal arteries and has shown that ACEI caused a significant decrease in GFR averaging ~26% in a group of kidneys with RAS 50% [99].

The effects of RVD on intrarenal hypoxia have been evaluated using BOLD MRI. Although it is relatively preserved in moderate RVD [100], a decrease renal oxygenation becomes evident once severe stenosis develops [4, 101]. This is possibly because in severe vascular occlusion that threatens cortical perfusion, processes of compensating tissue oxygenation become overwhelmed. Histogram-based analysis over large cortical and medullary regions can be used to evaluate the distribution of tissue oxygenation in these regions and reduces

sampling error [102]. Moreover, a furosemide challenge enables the study of tubular oxygen-dependent transport [103], which is blunted in damaged kidneys [104], but enhanced in hyper-filtering kidneys [105]. Hence, BOLD MRI may be useful to assess the functional integrity of the renal medullary tubules [106].

Other methods have also been explored in RVD. Magnetic resonance elastography (MRE) utilizes the translocation of mechanical shear waves to estimate elasticity, which may decrease in fibrotic kidneys. Interestingly, in swine with RVD overall kidney stiffness is unaltered, because a fall in RBF reduces renal turgor and masks decreased elasticity [107]. In contrast, medullary elasticity appears to be less dependent on hemodynamic variables, and may reflect kidney fibrosis [108].

DWI detects changes in tissue property based on its sensitivity to restriction of free-water diffusion. In patients with RVD [109], but not hypertension alone [110], apparent diffusion coefficient (ADC) declines and correlates with the extent of RVD, suggesting that significant kidney injury is required to become detectable by DWI.

The noninvasive and versatile nature of MRI positions this modality at the forefront for evaluation of RVD in humans. The rapid progress in this field will hopefully inspire the development of molecular and metabolic probes to assess mechanisms of injury and viability of the post-stenotic kidney. These developments would be for identifying the subset of patients with RVD who may benefit from revascularization of stenotic renal arteries [111]. The determination of tissue perfusion and oxygenation may facilitate the decision to perform the revascularization procedure and monitoring of the kidney responses after the procedure.

Diabetic Nephropathy (DN)

Recent advances suggest that progressive chronic kidney disease (CKD) eventually results in peritubular capillary injury, tubular hypoxia and atrophy, and interstitial fibrosis [112], independent of the type of underlying primary kidney disease. Diabetic nephropathy (DN) is the most common form of CKD, and functional renal MRI is an attractive opportunity for noninvasive diagnosis and monitoring of potential therapeutic interventions. Most studies have focused on hypoxia using BOLD MRI [113, 114], fibrosis using DWI, tubular damage using DTI [115, 116] or a combination of BOLD MRI and DWI [117, 118]. A recent preliminary report applied ASL to show reduced cortical blood flow in patients with CKD [81].

Studies using BOLD-MRI in rodent models suggest that, at least in the early stages, type 1 and type 2 diabetic nephropathy is associated with increased hypoxia [118–120]. DWI that measures water diffusion in the interstitial space, however, has failed to show any changes in early stage DN [118]. Part of the reason may be related to the specific parameters of the diffusion MRI method [121].

Clinical results of BOLD MRI in DN have been strikingly variable. Consistent with rodent studies, one recent BOLD MRI study of 46 patients with type 2 diabetes using 3.0 T MRI found that the ratios of medullary-to-cortical R_2* (MCR) were higher in stages 1 and 2 CKD compared to controls [114], suggesting a greater than expected medullary tissue hypoxia relative to the cortex. Interestingly the MCR values were lower at later stages (3–5) of CKD

compared to controls. The reason for this paradox is not apparent, but may provide interesting clues to understanding of the pathophysiology of DN. Another study of 20 diabetic patients (14 with stages 3–5 CKD) performed using 1.5 T MRI confirmed lower MCR values than healthy subjects [113]. Yet another study of type-2 diabetic patients (CKD stages 1–4) using 3.0 T MRI found no change in MCR compared to controls reported in the literature [122]. As noted above (BOLD section), the apparently contradictory results of BOLD imaging in these patients is likely due to technical challenges such as image artifacts and the oversimplification of interpretation of R_2^* (or T_2^*) values.

Diffusion-weighted imaging has also been applied to DN patients. A recent study of CKD patients with (n=43) or without (n=76) diabetes found a statistically significant correlation between ADC and estimated GFR values in both groups of patients [117]. However, this correlation was only seen in the non-diabetic patients and not in the diabetic patients. A recent DTI study suggested changes in fractional anisotropy in the renal medulla with different levels of DN [116] probably related to glomerulosclerosis, interstitial fibrosis, and tubular damage [115].

Overall, these reports clearly demonstrate the complexities involved in translating results from animal models to humans. In addition to technical challenges inherent in the MR methods, these discrepancies may also be related to differences species, pathogenesis of diabetes, severity of kidney disease, comorbid conditions, use of medications such as renin-angiotensin system blockers, hydration and other preparations for imaging. Further refinement and validation of these techniques and their applications to larger, well-designed clinical studies [114, 117] may establish their utility in clinical research of DN and routine clinical use.

Renal Transplants

MRI has emerged as an attractive approach for evaluating the function of renal allografts due to its noninvasiveness and suitability for repeated application. The most promising results have involved near-term allograft complications, of which acute tubular necrosis (ATN) and acute allograft rejection (AR) are the most common. Szolar et al. [123] observed that the first-pass cortical signal enhancement using DCE MRI was markedly reduced in allografts with AR compared to normally functioning kidneys, while allografts with ATN showed no difference compared to normal cases. Using a similar approach, Wentland et al. [124] reported lower cortical and medullary blood flow in AR compared to normal kidneys and lower medullary blood flow in AR compared to ATN. Most recently, by applying a multi-compartmental tracer kinetic model to DCE MR images, Yamamoto et al. [30] showed that mean transit times (MTT) could differentiate normal allografts from AR or ATN, where AR cases had higher ratio of vascular MTT over whole-kidney MTT while ATN cases had higher ratio of tubular MTT over whole-kidney MTT.

Several studies have investigated diagnosis of acute dysfunction using non-contrast techniques such as BOLD MRI. Sadowski et al. [125] and Han et al. [126] performed BOLD MRI in recent kidney transplant recipients and observed significantly lower medullary R_2^*, or higher oxygenation, in cases of AR compared to ATN. As the authors suggested, this could be due to preferential blood shunting toward the medulla during acute rejection or

reduced oxygen consumption rate due to subclinical medullary tubular injury or both. Together the results consistently show differentiation between ATN and AR based on perfusion and oxygenation parameters; however, robust differentiation of ATN from normally functioning allografts has not been demonstrated. Therefore, Chandarana et al. [6] have proposed a follow-up role for MRI only after acute dysfunction has been implicated by other tests such as elevated serum creatinine.

Studies of long-term allograft function have combined multiple functional MRI techniques, including BOLD, DWI and ASL MRI. In a cross-sectional BOLD MRI study of healthy volunteers and transplant recipients with chronic allograft nephropathy (CAN), Djamali et al. [127] observed significantly reduced cortical and medullary R_2*, indicating increased oxygenation, in allografts affected by CAN. Long-term longitudinal studies, however, have produced mixed results. Vermathen et al. [128] reported stable DWI parameters and an increase of cortical R_2* (decrease in oxygenation) in allografts between 7 and 32 months post-transplant. In a small pilot study involving matched donor and recipient pairs, Malvezzi et al. [129] observed a reduction in cortical R_2* in both groups and a reduction in medullary R_2* (increase in oxygenation) in the transplanted kidney 1 month following transplant. In a recent study of 14 donor and recipient pairs, Niles et al. [130] observed a reduction in both medullary R_2* (increase in oxygenation) and ASL-estimated cortical perfusion in transplanted kidneys 3 months post-transplant, and this reduction persisted for at least two years. The clinical significance of these changes was unclear, as all allografts were functioning well based on conventional clinical biomarkers. Further longitudinal studies with larger sample sizes will be necessary to determine whether long-term changes in MRI measures of allograft function are associated with clinical outcomes.

Renal Tumors

Renal masses are increasingly discovered incidentally, largely attributable to the increased use of medical imaging [131, 132]. Because tumors differ in biologic behavior, aggressiveness, and prognosis [133, 134], their increased detection has led to a management dilemma. Accurate characterization of tumor aggressiveness can guide management. Although CT is the most widely used to diagnose renal lesions in clinical practice, advantages of MRI include superior soft tissue contrast, avoidance of ionizing radiation and iodinated contrast media, and most importantly the availability of different techniques such as DCE, DWI and BOLD MRI to probe different aspects of tumor such as vascularity, microstructure and oxygenation (6).

Widely used clinically, DCE MRI is one of the most robust techniques for evaluating the aggressiveness of renal tumors [135, 136]. Studies have shown that by imaging at three time points following contrast administration, the low level and homogeneous enhancement of papillary renal cell carcinoma (RCC) can help distinguish it from clear cell RCC [137, 138]. With a higher temporal resolution of ~30 sec per acquisition, a distinct pattern of enhancement was identified for angiomyolipomas: an early enhancement peak followed by lower level enhancement [139]. Using a 2-compartmental model to analyze the high temporal resolution data, Notohamiprodio et al. [140] estimated perfusion and permeability of renal

tumors. These parameters could help differentiate tumor subtypes and identify tumor features such as necrosis and vessel invasion.

Cellular renal lesions, such as renal cell cancer (RCC), restrict water diffusion in interstitial space, which explains the associated lower ADC values in the lesion compared to normal tissue [141–143]. Kim et al. found significantly lower ADC values in malignant lesions compared to benign lesions (1.75 ± 0.57 vs. $2.50 \pm 0.53 \times 10^{-3}$ mm^2/sec) [144]. Sandrasegaran et al. [145] found similar results. Taouli et al. reported lower ADC values in Bosniak category 3 and 4 lesions compared to category 1 simple cysts, although a statistically significant difference between Bosniak 2F and 3–4 lesions was not detected [142]. Low ADC values have been shown in the papillary subtype of RCC compared to non papillary subtypes [142]. Wang et al. [146] found that clear cell RCCs showed a significantly higher mean ADC (1.85×10^{-3} mm^2/sec) than papillary (1.09×10^{-3} mm^2/sec) and chromophobe (1.31×10^{-3} mm^2/sec) RCCs. ADC has also been reported to be significantly lower in high nuclear grade (III and IV) than low nuclear grade (I&II) clear cell RCCs [147]. With advanced DWI methods, Chandarana et al. showed that DWI has potential in assessing renal tumor cellularity as well as vascularity, and can help discriminate RCC subtypes [148, 149].

Acute Kidney Injury (AKI)

AKI, previously termed as acute renal failure, refers to a rapid and reversible decline of GFR within days or weeks and has recently been defined and classified more specifically by the RIFLE (risk, injury, failure, loss, end stage) criteria [150, 151]. Causes of AKI include renal ischemia and renal parenchymal diseases such as contrast-induced nephropathy (CIN) and acute tubular necrosis (ATN). AKI predisposes the patients to chronic kidney diseases [152, 153].

Although DCE MRI with low Gd dose is capable of measuring single-kidney GFR with higher accuracy than serum creatinine, it is typically not used for assessing AKI as lowered GFR in severe AKI patients could potentially increase the risk of NSF. He et al. [154] developed an innovative non-contrast MRI technique for estimating GFR based on ASL. Although not yet validated against any gold standard, this approach showed a promising 28% increase in the estimated GFR after protein loading, as would be expected. In a rat model of ischemic AKI, Zimmer et al [155] observed that although their ASL-estimated cortical perfusion was ~30% lower than that from DCE MRI, both were able to differentiate between healthy and AKI cases. Prowle et al. [156] used phase-contrast MRI, a non-contrast MRI method to measure blood flow rate through the renal artery, and found that RBF in ischemic AKI patients was significantly lower than that in normal volunteers (335–1137 ml/min vs. 791–1750 mL/min).

Tissue oxygenation is another physiologic parameter of interest for AKI [157, 158]. BOLD MRI enables non-invasive mapping of renal tissue oxygenation for human subjects (section "BOLD MRI"). Assessment of acute tubular necrosis by BOLD is also discussed in section "Renal Transplants". Contrast induced nephropathy (CIN) is another form of AKI. Using BOLD and a rat model of CIN, Li et al. [159] found that BOLD measurements could detect the effects of viscosity and dose of iodinated contrast on subsequent CIN.

Pediatric Kidney Imaging

Congenital anomalies of the kidney and urinary tract are frequent in children. Ultrasonography remains the primary imaging modality to image these disorders. An extension of MRR, MR urography (Figure 5) is increasingly used in practice as a complementary tool since it can combine exquisite anatomic depiction and functional evaluation in a single examination without radiation exposure. Heavily T_2 weighted images allow a complete visualization of the urinary tract in a few seconds (with 2D acquisitions) to few minutes (with 3D acquisitions and respiratory synchronization). With 3D isotropic acquisitions, multiplanar and volumetric reconstructions that are easily understandable for urologists have made intravenous urography obsolete. Additionally, the renal parenchyma can be studied in detail: corticomedullary differentiation, thickness, cortical scarring, and cysts.

In pediatric urology, one of the most challenging issues is to identify whether dilated systems have true obstruction and therefore require surgery. True chronic obstruction is defined in practice by a decrease in the split (differential) renal function (SRF) on serial functional imaging, such as renal scintigraphy, MRR or MR urography [160–162]. Using gadolinium contrast agents and a tracer compartmental model of analysis, the relative filtration of the parenchyma can be calculated for each side with classical scintigraphic-derived estimates such as the integral method and/or the Rutland-Patlak method [32, 163, 164]. These results have to take into account the volume of renal parenchyma on both sides. As with scintigraphy, many estimates have been developed to assess the drainage such as the shape of the renograms or transit times [165, 166]. These parameters turned out to be of poor value, and the presence of chronic obstruction remains based on an evolving decrease in SRF.

Conclusion

With high diagnostic reliability, anatomic MRI of the kidneys and their blood vessels has achieved widespread clinical adoption. On the other hand, the functional MRI techniques for the kidneys require more work for their clinical application. Of the functional methods available, the low-dose gadolinium-enhanced imaging (MR renography or MR urography) are closest to clinical adoption. In pediatrics, these methods have been proven to be useful for determining functional obstruction in the setting of hydronephrosis or ureterectasis. In both pediatrics and adults, numerous studies have validated the high agreement between the glomerular filtration of gadolinium chelates as a marker of GFR and other more established techniques. Among the other functional methods, BOLD imaging promises the most valuable insights into renal disease with the opportunity to measure hypoxia noninvasively. Addressing technical challenges for BOLD is the focus of many laboratories, and it is likely that in addition to improving acquisition techniques for reducing image artifacts, the development of appropriate physiologic models to interpret the BOLD data will be critical. The jury is still out on methods such as ASL and DWI, both of which have either technical challenges or image interpretation issues. Given the prevalence and growing rate of renal diseases together with MRI's advantages of providing both high resolution anatomic imaging without exposure to ionizing radiation, functional renal MRI is worthy of intensive

research effort which will be most successful where nephrologists and urologists collaborate with radiologists and MR scientists.

References

1. Lee VS, Rusinek H, Johnson G, et al. MR renography with low-dose gadopentetate dimeglumine: feasibility. Radiology. 2001; 221:371–379. [PubMed: 11687678]

2. Lee VS, Rusinek H, Bokacheva L, et al. Renal function measurements from MR renography and a simplified multicompartmental model. American journal of physiology. 2007; 292:F1548–F1559. [PubMed: 17213464]

3. Prasad PV, Edelman RR, Epstein FH. Noninvasive evaluation of intrarenal oxygenation with BOLD MRI. Circulation. 1996; 94:3271–3275. [PubMed: 8989140]

4. Textor SC, Glockner JF, Lerman LO, et al. The use of magnetic resonance to evaluate tissue oxygenation in renal artery stenosis. J Am Soc Nephrol. 2008; 19:780–788. [PubMed: 18287564]

5. Prasad PV. Functional MRI of the kidney: tools for translational studies of pathophysiology of renal disease. American journal of physiology. 2006; 290:F958–F974. [PubMed: 16601297]

6. Chandarana H, Lee VS. Renal functional MRI: Are we ready for clinical application? AJR Am J Roentgenol. 2009; 192:1550–1557. [PubMed: 19457818]

7. Grenier N, Basseau F, Ries M, et al. Functional MRI of the kidney. Abdom Imaging. 2003; 28:164–175. [PubMed: 12592462]

8. Kalb B, Martin DR, Salman K, et al. Kidney transplantation: structural and functional evaluation using MR Nephro-Urography. J Magn Reson Imaging. 2008; 28:805–822. [PubMed: 18821623]

9. Nikken JJ, Krestin GP. MRI of the kidney-state of the art. Eur Radiol. 2007; 17:2780–2793. [PubMed: 17646992]

10. Li LP, Halter S, Prasad PV. Blood Oxygen Level-Dependent MR Imaging of the Kidneys. Magnetic resonance imaging clinics of North America. 2008; 16:613–625. [PubMed: 18926426]

11. Attenberger UI, Morelli JN, Schoenberg SO, et al. Assessment of the kidneys: magnetic resonance angiography, perfusion and diffusion. J Cardiovasc Magn Reson. 2011; 13:70. [PubMed: 22085467]

12. Artunc F, Rossi C, Boss A. MRI to assess renal structure and function. Current opinion in nephrology and hypertension. 2011; 20:669–675. [PubMed: 21885971]

13. Notohamiprodjo M, Reiser MF, Sourbron SP. Diffusion and perfusion of the kidney. European journal of radiology. 2010; 76:337–347. [PubMed: 20580179]

14. Liss P, Cox EF, Eckerbom P, et al. Imaging of intrarenal haemodynamics and oxygen metabolism. Clinical and experimental pharmacology & physiology. 2013; 40:158–167. [PubMed: 23252679]

15. Grobner T. Gadolinium--a specific trigger for the development of nephrogenic fibrosing dermopathy and nephrogenic systemic fibrosis? Nephrol Dial Transplant. 2006; 21:1104–1108. [PubMed: 16431890]

16. Leiner T, Kucharczyk W. NSF prevention in clinical practice: summary of recommendations and guidelines in the United States, Canada, and Europe. J Magn Reson Imaging. 2009; 30:1357–1363. [PubMed: 19937935]

17. Thomsen HS. ESUR guideline: gadolinium-based contrast media and nephrogenic systemic fibrosis. Eur Radiol. 2007; 17:2692–2696. [PubMed: 17977076]

18. Wang Y, Alkasab TK, Narin O, et al. Incidence of nephrogenic systemic fibrosis after adoption of restrictive gadolinium-based contrast agent guidelines. Radiology. 2011; 260:105–111. [PubMed: 21586680]

19. Bokacheva L, Rusinek H, Chen Q, et al. Quantitative determination of Gd-DTPA concentration in T(1)-weighted MR renography studies. Magn Reson Med. 2007; 57:1012–1018. [PubMed: 17534906]

20. Donahue KM, Weisskoff RM, Burstein D. Water diffusion and exchange as they influence contrast enhancement. J Magn Reson Imaging. 1997; 7:102–110. [PubMed: 9039599]

21. Zhang JL, Rusinek H, Bokacheva L, et al. Functional assessment of the kidney from magnetic resonance and computed tomography renography: impulse retention approach to a multicompartment model. Magn Reson Med. 2008; 59:278–288. [PubMed: 18228576]

22. Sourbron SP, Michaely HJ, Reiser MF, et al. MRI-measurement of perfusion and glomerular filtration in the human kidney with a separable compartment model. Investigative radiology. 2008; 43:40–48. [PubMed: 18097276]

23. Buckley DL, Shurrab AE, Cheung CM, et al. Measurement of single kidney function using dynamic contrast-enhanced MRI: comparison of two models in human subjects. J Magn Reson Imaging. 2006; 24:1117–1123. [PubMed: 16941606]

24. Bokacheva L, Rusinek H, Zhang JL, et al. Estimates of glomerular filtration rate from MR renography and tracer kinetic models. J Magn Reson Imaging. 2009; 29:371–382. [PubMed: 19161190]

25. Tofts PS, Cutajar M, Mendichovszky IA, et al. Precise measurement of renal filtration and vascular parameters using a two-compartment model for dynamic contrast-enhanced MRI of the kidney gives realistic normal values. Eur Radiol. 2012; 22:1320–1330. [PubMed: 22415410]

26. Hackstein N, Kooijman H, Tomaselli S, et al. Glomerular filtration rate measured using the Patlak plot technique and contrast-enhanced dynamic MRI with different amounts of gadolinium-DTPA. J Magn Reson Imaging. 2005; 22:406–414. [PubMed: 16106358]

27. Cutajar M, Mendichovszky IA, Tofts PS, et al. The importance of AIF ROI selection in DCE-MRI renography: reproducibility and variability of renal perfusion and filtration. European journal of radiology. 2010; 74:e154–e160. [PubMed: 19541441]

28. Zhang JL, Rusinek H, Bokacheva L, et al. Use of cardiac output to improve measurement of input function in quantitative dynamic contrast-enhanced MRI. J Magn Reson Imaging. 2009; 30:656–665. [PubMed: 19711414]

29. Park JB, Hu BS, Conolly SM, et al. Rapid cardiac-output measurement with ungated spiral phase contrast. Magn Reson Med. 2006; 56:432–438. [PubMed: 16802317]

30. Yamamoto A, Zhang JL, Rusinek H, et al. Quantitative evaluation of acute renal transplant dysfunction with low-dose three-dimensional MR renography. Radiology. 2011; 260:781–789. [PubMed: 21771953]

31. Khrichenko D, Darge K. Functional analysis in MR urography - made simple. Pediatr Radiol. 2010; 40:182–199. [PubMed: 20012602]

32. Vivier PH, Dolores M, Taylor M, et al. MR urography in children. Part 2: how to use ImageJ MR urography processing software. Pediatr Radiol. 2010; 40:739–746. [PubMed: 20182707]

33. Mikheev, AL.; V.S.; Rusinek, H., editors. Targeted coregistration of abdominal DCE MRI; Proceedings of he Conference Name; Date Year of Conference; Conference Location|. Publisher|: Place Published|, Year Published|.

34. Rusinek H, Boykov Y, Kaur M, et al. Performance of an automated segmentation algorithm for 3D MR renography. Magn Reson Med. 2007; 57:1159–1167. [PubMed: 17534915]

35. Ogawa S, Lee TM, Kay AR, et al. Brain magnetic resonance imaging with contrast dependent on blood oxygenation. Proc Natl Acad Sci U S A. 1990; 87:9868–9872. [PubMed: 2124706]

36. Brezis M, Agmon Y, Epstein FH. Determinants of intrarenal oxygenation. I. Effects of diuretics. Am J Physiol. 1994; 267:F1059–F1062. [PubMed: 7810692]

37. Warner L, Glockner JF, Woollard J, et al. Determinations of renal cortical and medullary oxygenation using blood oxygen level-dependent magnetic resonance imaging and selective diuretics. Invest Radiol. 2011; 46:41–47. [PubMed: 20856128]

38. Priatna A, Epstein FH, Spokes K, et al. Evaluation of changes in intrarenal oxygenation in rats using multiple gradient-recalled echo (mGRE) sequence. J Magn Reson Imaging. 1999; 9:842–846. [PubMed: 10373033]

39. Economides PA, Caselli A, Zuo CS, et al. Kidney oxygenation during water diuresis and endothelial function in patients with type 2 diabetes and subjects at risk to develop diabetes. Metabolism. 2004; 53:222–227. [PubMed: 14767875]

40. Epstein FH, Veves A, Prasad PV. Effect of diabetes on renal medullary oxygenation during water diuresis. Diabetes Care. 2002; 25:575–578. [PubMed: 11874950]

41. Epstein FH, Prasad P. Effects of furosemide on medullary oxygenation in younger and older subjects. Kidney Int. 2000; 57:2080–2083. [PubMed: 10792627]

42. Yin WJ, Liu F, Li XM, et al. Noninvasive evaluation of renal oxygenation in diabetic nephropathy by BOLD-MRI. Eur J Radiol. 2012; 81:1426–1431. [PubMed: 21470811]

43. dos Santos EA, Li LP, Ji L, et al. Early changes with diabetes in renal medullary hemodynamics as evaluated by fiberoptic probes and BOLD magnetic resonance imaging. Invest Radiol. 2007; 42:157–162. [PubMed: 17287645]

44. Fine LG, Bandyopadhay D, Norman JT. Is there a common mechanism for the progression of different types of renal diseases other than proteinuria? Towards the unifying theme of chronic hypoxia. Kidney international Supplement. 2000; 75:S22–S26. [PubMed: 10828757]

45. Fine LG, Norman JT. Chronic hypoxia as a mechanism of progression of chronic kidney diseases: from hypothesis to novel therapeutics. Kidney Int. 2008; 74:867–872. [PubMed: 18633339]

46. Nangaku M. Chronic hypoxia and tubulointerstitial injury: a final common pathway to end-stage renal failure. J Am Soc Nephrol. 2006; 17:17–25. [PubMed: 16291837]

47. Michaely HJ, Metzger L, Haneder S, et al. Renal BOLD-MRI does not reflect renal function in chronic kidney disease. Kidney Int. 2012; 81:684–689. [PubMed: 22237750]

48. Ries M, Basseau F, Tyndal B, et al. Renal diffusion and BOLD MRI in experimental diabetic nephropathy. Blood oxygen level-dependent. J Magn Reson Imaging. 2003; 17:104–113. [PubMed: 12500279]

49. Morrell, G.; Jeong, EK.; Shi, X., et al. Proceedings of the 21th Annual Meeting of ISMRM. Salt Lake City, USA: 2013. Prospectively navigated multi-echo GRE sequence for improved 2D BOLD imaging of the kidneys; p. 1569

50. Zhang, JL.; Warner, L.; Rusinek, H., et al. Proceedings of the 19th Annual Meeting of ISMRM. Montreal, Canada: 2011. Establishment of a renal oxygen transit model based on BOLD MRI; p. 442

51. Zhang, JL.; H, R.; H, C., et al. Proceedings of the 18th Annual Meeting of ISMRM. Stockholm, Sweden: 2010. Functional renal imaging with BOLD: validation of a model for R2* in kidney cortex and medulla; p. 4681

52. Glover GH. 3D z-shim method for reduction of susceptibility effects in BOLD fMRI. Magn Reson Med. 1999; 42:290–299. [PubMed: 10440954]

53. Detre JA, Leigh JS, Williams DS, et al. Perfusion imaging. Magn Reson Med. 1992; 23:37–45. [PubMed: 1734182]

54. Williams DS, Detre JA, Leigh JS, et al. Magnetic resonance imaging of perfusion using spin inversion of arterial water. Proc Natl Acad Sci U S A. 1992; 89:212–216. [PubMed: 1729691]

55. Martirosian P, Klose U, Mader I, et al. FAIR true-FISP perfusion imaging of the kidneys. Magn Reson Med. 2004; 51:353–361. [PubMed: 14755661]

56. Grossman EJ, Zhang K, An J, et al. Measurement of deep gray matter perfusion using a segmented true-fast imaging with steady-state precession (True-FISP) arterial spin-labeling (ASL) method at 3T. J Magn Reson Imaging. 2009; 29:1425–1431. [PubMed: 19472418]

57. Marckmann P, Skov L, Rossen K, et al. Nephrogenic systemic fibrosis: suspected causative role of gadodiamide used for contrast-enhanced magnetic resonance imaging. J Am Soc Nephrol. 2006; 17:2359–2362. [PubMed: 16885403]

58. Sadowski EA, Bennett LK, Chan MR, et al. Nephrogenic systemic fibrosis: risk factors and incidence estimation. Radiology. 2007; 243:148–157. [PubMed: 17267695]

59. Kuo PH, Kanal E, Abu-Alfa AK, et al. Gadolinium-based MR contrast agents and nephrogenic systemic fibrosis. Radiology. 2007; 242:647–649. [PubMed: 17213364]

60. Artz NS, Sadowski EA, Wentland AL, et al. Arterial spin labeling MRI for assessment of perfusion in native and transplanted kidneys. Magn Reson Imaging. 2011; 29:74–82. [PubMed: 20850241]

61. Robson PM, Madhuranthakam AJ, Dai W, et al. Strategies for reducing respiratory motion artifacts in renal perfusion imaging with arterial spin labeling. Magn Reson Med. 2009; 61:1374–1387. [PubMed: 19319891]

62. Tan H, Koktzoglou I, Prasad PV. Renal perfusion imaging with two-dimensional navigator gated arterial spin labeling. Magn Reson Med. 2013 Feb 27. [Epub ahead of print].

63. Gardener AG, Francis ST. Multislice perfusion of the kidneys using parallel imaging: image acquisition and analysis strategies. Magn Reson Med. 2010; 63:1627–1636. [PubMed: 20512866]

64. Artz NS, Sadowski EA, Wentland AL, et al. Reproducibility of renal perfusion MR imaging in native and transplanted kidneys using non-contrast arterial spin labeling. J Magn Reson Imaging. 2011; 33:1414–1421. [PubMed: 21591011]

65. Artz NS, Wentland AL, Sadowski EA, et al. Comparing kidney perfusion using noncontrast arterial spin labeling MRI and microsphere methods in an interventional swine model. Investigative radiology. 2011; 46:124–131. [PubMed: 22609830]

66. Boss A, Martirosian P, Graf H, et al. High resolution MR perfusion imaging of the kidneys at 3 Tesla without administration of contrast media. Rofo. 2005; 177:1625–1630. [PubMed: 16333784]

67. de Bazelaire C, Alsop DC, George D, et al. Magnetic resonance imaging-measured blood flow change after antiangiogenic therapy with PTK787/ZK 222584 correlates with clinical outcome in metastatic renal cell carcinoma. Clinical cancer research : an official journal of the American Association for Cancer Research. 2008; 14:5548–5554. [PubMed: 18765547]

68. De Bazelaire C, Rofsky NM, Duhamel G, et al. Arterial spin labeling blood flow magnetic resonance imaging for the characterization of metastatic renal cell carcinoma(1). Academic radiology. 2005; 12:347–357. [PubMed: 15766695]

69. Fenchel M, Martirosian P, Langanke J, et al. Perfusion MR imaging with FAIR true FISP spin labeling in patients with and without renal artery stenosis: initial experience. Radiology. 2006; 238:1013–1021. [PubMed: 16439565]

70. Heusch P, Wittsack HJ, Heusner T, et al. Correlation of biexponential diffusion parameters with arterial spin-labeling perfusion MRI: results in transplanted kidneys. Investigative radiology. 2013; 48:140–144. [PubMed: 23249648]

71. Karger N, Biederer J, Lusse S, et al. Quantitation of renal perfusion using arterial spin labeling with FAIR-UFLARE. Magn Reson Imaging. 2000; 18:641–647. [PubMed: 10930773]

72. Lanzman RS, Robson PM, Sun MR, et al. Arterial spin-labeling MR imaging of renal masses: correlation with histopathologic findings. Radiology. 2012; 265:799–808. [PubMed: 23047841]

73. Lanzman RS, Wittsack HJ, Martirosian P, et al. Quantification of renal allograft perfusion using arterial spin labeling MRI: initial results. Eur Radiol. 2009; 20:1485–1491. [PubMed: 19949799]

74. Michaely HJ, Schoenberg SO, Ittrich C, et al. Renal disease: value of functional magnetic resonance imaging with flow and perfusion measurements. Invest Radiol. 2004; 39:698–705. [PubMed: 15486531]

75. Pedrosa I, Rafatzand K, Robson P, et al. Arterial spin labeling MR imaging for characterisation of renal masses in patients with impaired renal function: initial experience. Eur Radiol. 2012; 22:484–492. [PubMed: 21877173]

76. Ritt M, Janka R, Schneider MP, et al. Measurement of kidney perfusion by magnetic resonance imaging: comparison of MRI with arterial spin labeling to para-aminohippuric acid plasma clearance in male subjects with metabolic syndrome. Nephrol Dial Transplant. 2009; 25:1126–1133. [PubMed: 19934080]

77. Roberts DA, Detre JA, Bolinger L, et al. Renal perfusion in humans: MR imaging with spin tagging of arterial water. Radiology. 1995; 196:281–286. [PubMed: 7784582]

78. Rossi C, Artunc F, Martirosian P, et al. Histogram analysis of renal arterial spin labeling perfusion data reveals differences between volunteers and patients with mild chronic kidney disease. Invest Radiol. 2012; 47:490–496. [PubMed: 22766911]

79. Sugimori H, Nakanishi M, Fujima N, et al. Evaluation of renal blood flow using multi-phase echoplanar magnetic resonance imaging and signal targeting with alternating radiofrequency (EPISTAR) in 3-T magnetic resonance imaging. Radiological physics and technology. 2013; 6:86–91. [PubMed: 22869501]

80. Wu WC, Su MY, Chang CC, et al. Renal Perfusion 3-T MR Imaging: A Comparative Study of Arterial Spin Labeling and Dynamic Contrast-enhanced Techniques. Radiology. 2011; 261:845–853. [PubMed: 22095996]

81. Tan H, Koktzoglou I, Prasad PV. Renal perfusion imaging with two-dimensional navigator gated arterial spin labeling. Magn Reson Med. 2013

82. Petersen ET, Zimine I, Ho YC, et al. Non-invasive measurement of perfusion: a critical review of arterial spin labelling techniques. Br J Radiol. 2006; 79:688–701. [PubMed: 16861326]

83. Wu WC, Fernandez-Seara M, Detre JA, et al. A theoretical and experimental investigation of the tagging efficiency of pseudocontinuous arterial spin labeling. Magn Reson Med. 2007; 58:1020–1027. [PubMed: 17969096]

84. Basser PJ, Pierpaoli C. Microstructural and physiological features of tissues elucidated by quantitative-diffusion-tensor MRI. Journal of Magnetic Resonance Series B. 1996; 111:209–219. [PubMed: 8661285]

85. Basser PJ, Mattiello J, Lebihan D. Mr Diffusion Tensor Spectroscopy and Imaging. Biophys J. 1994; 66:259–267. [PubMed: 8130344]

86. Gurses B, Kilickesmez O, Tasdelen N, et al. Diffusion tensor imaging of the kidney at 3 Tesla MRI: normative values and repeatability of measurements in healthy volunteers. Diagnostic and interventional radiology (Ankara, Turkey). 2011; 17:317–322.

87. Kido A, Kataoka M, Yamamoto A, et al. Diffusion tensor MRI of the kidney at 3.0 and 1.5 Tesla. Acta Radiol. 2010; 51:1059–1063. [PubMed: 20735277]

88. Lebihan D, Breton E, Lallemand D, et al. Separation of Diffusion and Perfusion in Intravoxel Incoherent Motion Mr Imaging. Radiology. 1988; 168:497–505. [PubMed: 3393671]

89. Xu Y, Wang X, Jiang X. Relationship between the renal apparent diffusion coefficient and glomerular filtration rate: preliminary experience. J Magn Reson Imaging. 2007; 26:678–681. [PubMed: 17729335]

90. Sigmund, EE.; Jensen, JH. Basic physical principles of body diffusion-weighted imaging. In: Taouli, B., editor. Extra-Cranial Applications of Diffusion-Weighted MRI. Cambridge University Press; 2011. p. 1-17.

91. Thoeny HC, De Keyzer F, Oyen RH, et al. Diffusion-weighted MR imaging of kidneys in healthy volunteers and patients with parenchymal diseases: initial experience. Radiology. 2005; 235:911–917. [PubMed: 15845792]

92. Sigmund EE, Vivier PH, Sui D, et al. Intravoxel incoherent motion and diffusion-tensor imaging in renal tissue under hydration and furosemide flow challenges. Radiology. 2012; 263:758–769. [PubMed: 22523327]

93. Lee VS, Rofsky NM, Krinsky GA, et al. Single-dose breath-hold gadolinium-enhanced threedimensional MR angiography of the renal arteries. Radiology. 1999; 211:69–78. [PubMed: 10189455]

94. Miyazaki M, Lee VS. Nonenhanced MR angiography. Radiology. 2008; 248:20–43. [PubMed: 18566168]

95. Prince MR, Schoenberg SO, Ward JS, et al. Hemodynamically significant atherosclerotic renal artery stenosis: MR angiographic features. Radiology. 1997; 205:128–136. [PubMed: 9314974]

96. Schoenberg SO, Aumann S, Just A, et al. Quantification of renal perfusion abnormalities using an intravascular contrast agent (part 2): results in animals and humans with renal artery stenosis. Magn Reson Med. 2003; 49:288–298. [PubMed: 12541249]

97. Schoenberg SO, Rieger JR, Michaely HJ, et al. Functional magnetic resonance imaging in renal artery stenosis. Abdom Imaging. 2006; 31:200–212. [PubMed: 16317490]

98. Prasad PV, Goldfarb J, Sundaram C, et al. Captopril MR renography in a swine model: toward a comprehensive evaluation of renal arterial stenosis. Radiology. 2000; 217:813–818. [PubMed: 11110948]

99. Zhang JL, Rusinek H, Bokacheva L, et al. Angiotensin-converting enzyme inhibitor-enhanced MR renography: repeated measures of GFR and RPF in hypertensive patients. American journal of physiology. 2009; 296:F884–F891. [PubMed: 19158343]

100. Gloviczki ML, Glockner JF, Lerman LO, et al. Preserved oxygenation despite reduced blood flow in poststenotic kidneys in human atherosclerotic renal artery stenosis. Hypertension. 2010; 55:961–966. [PubMed: 20194303]

101. Gloviczki ML, Glockner JF, Crane JA, et al. Blood oxygen level-dependent magnetic resonance imaging identifies cortical hypoxia in severe renovascular disease. Hypertension. 2011; 58:1066–1072. [PubMed: 22042812]

102. Ebrahimi B, Gloviczki M, Woollard JR, et al. Compartmental analysis of renal BOLD MRI data: introduction and validation. Investigative radiology. 2012; 47:175–182. [PubMed: 22183077]

103. Warner L, Glockner JF, Woollard J, et al. Determinations of renal cortical and medullary oxygenation using blood oxygen level-dependent magnetic resonance imaging and selective diuretics. Invest Radiol. 2011; 46:41–47. [PubMed: 20856128]

104. Gloviczki ML, Keddis MT, Garovic VD, et al. TGF Expression and Macrophage Accumulation in Atherosclerotic Renal Artery Stenosis. Clin J Am Soc Nephrol. 2012

105. Textor SC, Gloviczki ML, Flessner MF, et al. Association of filtered sodium load with medullary volumes and medullary hypoxia in hypertensive african americans as compared with whites. Am J Kidney Dis. 2012; 59:229–237. [PubMed: 22130642]

106. Eirin A, Ebrahimi B, Zhang X, et al. Changes in glomerular filtration rate after renal revascularization correlate with microvascular hemodynamics and inflammation in Swine renal artery stenosis. Circ Cardiovasc Interv. 2012; 5:720–728. [PubMed: 23048054]

107. Warner L, Yin M, Glaser KJ, et al. Noninvasive In Vivo Assessment of Renal Tissue Elasticity During Graded Renal Ischemia Using MR Elastography. Invest Radiol. 2011; 46:509–514. [PubMed: 21467945]

108. Korsmo MJ, Ebrahimi B, Eirin A, et al. Magnetic resonance elastography noninvasively detects in vivo renal medullary fibrosis secondary to Swine renal artery stenosis. Invest Radiol. 2013; 48:61–68. [PubMed: 23262789]

109. Yildirim E, Kirbas I, Teksam M, et al. Diffusion-weighted MR imaging of kidneys in renal artery stenosis. European journal of radiology. 2008; 65:148–153. [PubMed: 17537606]

110. Yildirim E, Gullu H, Caliskan M, et al. The effect of hypertension on the apparent diffusion coefficient values of kidneys. Diagnostic and interventional radiology (Ankara, Turkey). 2008; 14:9–13.

111. Murphy TP, Cooper CJ, Dworkin LD, et al. The Cardiovascular Outcomes with Renal Atherosclerotic Lesions (CORAL) study: rationale and methods. J Vasc Interv Radiol. 2005; 16:1295–1300. [PubMed: 16221898]

112. Fine LG, Norman JT. Chronic hypoxia as a mechanism of progression of chronic kidney diseases: from hypothesis to novel therapeutics. Kidney international. 2008; 74:867–872. [PubMed: 18633339]

113. Wang ZJ, Kumar R, Banerjee S, et al. Blood oxygen level-dependent (BOLD) MRI of diabetic nephropathy: preliminary experience. J Magn Reson Imaging. 2011; 33:655–660. [PubMed: 21563249]

114. Yin WJ, Liu F, Li XM, et al. Noninvasive evaluation of renal oxygenation in diabetic nephropathy by BOLD-MRI. European journal of radiology. 2012; 81:1426–1431. [PubMed: 21470811]

115. Hueper K, Hartung D, Gutberlet M, et al. Magnetic resonance diffusion tensor imaging for evaluation of histopathological changes in a rat model of diabetic nephropathy. Investigative radiology. 2012; 47:430–437. [PubMed: 22659594]

116. Lu L, Sedor JR, Gulani V, et al. Use of diffusion tensor MRI to identify early changes in diabetic nephropathy. American journal of nephrology. 2011; 34:476–482. [PubMed: 22024476]

117. Inoue T, Kozawa E, Okada H, et al. Noninvasive evaluation of kidney hypoxia and fibrosis using magnetic resonance imaging. J Am Soc Nephrol. 2011; 22:1429–1434. [PubMed: 21757771]

118. Ries M, Basseau F, Tyndal B, et al. Renal diffusion and BOLD MRI in experimental diabetic nephropathy. Blood oxygen level-dependent. Journal of magnetic resonance imaging : JMRI. 2003; 17:104–113. [PubMed: 12500279]

119. dos Santos EA, Li LP, Ji L, et al. Early changes with diabetes in renal medullary hemodynamics as evaluated by fiberoptic probes and BOLD magnetic resonance imaging. Investigative radiology. 2007; 42:157–162. [PubMed: 17287645]

120. Prasad P, Li LP, Halter S, et al. Evaluation of renal hypoxia in diabetic mice by BOLD MRI. Investigative radiology. 2010; 45:819–822. [PubMed: 20829708]

121. Togao O, Doi S, Kuro-o M, et al. Assessment of renal fibrosis with diffusion-weighted MR imaging: study with murine model of unilateral ureteral obstruction. Radiology. 2010; 255:772–780. [PubMed: 20406881]

122. Pruijm M, Hofmann L, Zanchi A, et al. Blockade of the renin-angiotensin system and renal tissue oxygenation as measured with BOLD-MRI in patients with type 2 diabetes. Diabetes research and clinical practice. 2012

123. Szolar DH, Preidler K, Ebner F, et al. Functional magnetic resonance imaging of human renal allografts during the post-transplant period: preliminary observations. Magn Reson Imaging. 1997; 15:727–735. [PubMed: 9309603]

124. Wentland AL, Sadowski EA, Djamali A, et al. Quantitative MR measures of intrarenal perfusion in the assessment of transplanted kidneys: initial experience. Academic radiology. 2009; 16:1077–1085. [PubMed: 19539502]

125. Sadowski EA, Fain SB, Alford SK, et al. Assessment of acute renal transplant rejection with blood oxygen level-dependent MR imaging: initial experience. Radiology. 2005; 236:911–919. [PubMed: 16118170]

126. Han F, Xiao W, Xu Y, et al. The significance of BOLD MRI in differentiation between renal transplant rejection and acute tubular necrosis. Nephrol Dial Transplant. 2008; 23:2666–2672. [PubMed: 18308769]

127. Djamali A, Sadowski EA, Muehrer RJ, et al. BOLD-MRI assessment of intrarenal oxygenation and oxidative stress in patients with chronic kidney allograft dysfunction. American journal of physiology. 2007; 292:F513–F522. [PubMed: 17062846]

128. Vermathen P, Binser T, Boesch C, et al. Three-year follow-up of human transplanted kidneys by diffusion-weighted MRI and blood oxygenation level-dependent imaging. J Magn Reson Imaging. 2012; 35:1133–1138. [PubMed: 22180302]

129. Malvezzi P, Bricault I, Terrier N, et al. Evaluation of intrarenal oxygenation by blood oxygen level-dependent magnetic resonance imaging in living kidney donors and their recipients: preliminary results. Transplantation proceedings. 2009; 41:641–644. [PubMed: 19328943]

130. Niles, DJ.; Artz, NS.; Sadowski, E., et al. Proceedings of the 20th Annual Meeting of ISMRM. Melbourne, Australia: 2012. Longitudinal measurement of renal oxygenation and perfusion in donor-recipient pairs using BOLD and ASL MRI. (abstract 0341)

131. Jayson M, Sanders H. Increased incidence of serendipitously discovered renal cell carcinoma. Urology. 1998; 51:203–205. [PubMed: 9495698]

132. Chow WH, Devesa SS, Warren JL, et al. Rising incidence of renal cell cancer in the United States. Jama. 1999; 281:1628–1631. [PubMed: 10235157]

133. Lam JS, Shvarts O, Leppert JT, et al. Renal cell carcinoma 2005: new frontiers in staging, prognostication and targeted molecular therapy. The Journal of urology. 2005; 173:1853–1862. [PubMed: 15879764]

134. Cheville JC, Lohse CM, Zincke H, et al. Comparisons of outcome and prognostic features among histologic subtypes of renal cell carcinoma. The American journal of surgical pathology. 2003; 27:612–624. [PubMed: 12717246]

135. Ho VB, Allen SF, Hood MN, et al. Renal masses: quantitative assessment of enhancement with dynamic MR imaging. Radiology. 2002; 224:695–700. [PubMed: 12202701]

136. Hecht EM, Israel GM, Krinsky GA, et al. Renal masses: quantitative analysis of enhancement with signal intensity measurements versus qualitative analysis of enhancement with image subtraction for diagnosing malignancy at MR imaging. Radiology. 2004; 232:373–378. [PubMed: 15215544]

137. Sun MR, Ngo L, Genega EM, et al. Renal cell carcinoma: dynamic contrast-enhanced MR imaging for differentiation of tumor subtypes--correlation with pathologic findings. Radiology. 2009; 250:793–802. [PubMed: 19244046]

138. Chandarana H, Rosenkrantz AB, Mussi TC, et al. Histogram analysis of whole-lesion enhancement in differentiating clear cell from papillary subtype of renal cell cancer. Radiology. 2012; 265:790–798. [PubMed: 23175544]

139. Scialpi M, Di Maggio A, Midiri M, et al. Small renal masses: assessment of lesion characterization and vascularity on dynamic contrast-enhanced MR imaging with fat suppression. AJR Am J Roentgenol. 2000; 175:751–757. [PubMed: 10954462]

140. Notohamiprodjo M, Sourbron S, Staehler M, et al. Measuring perfusion and permeability in renal cell carcinoma with dynamic contrast-enhanced MRI: a pilot study. J Magn Reson Imaging. 2010; 31:490–501. [PubMed: 20099364]

141. Cova M, Squillaci E, Stacul F, et al. Diffusion-weighted MRI in the evaluation of renal lesions: preliminary results. Br J Radiol. 2004; 77:851–857. [PubMed: 15482997]

142. Taouli B, Thakur RK, Mannelli L, et al. Renal lesions: characterization with diffusion-weighted imaging versus contrast-enhanced MR imaging. Radiology. 2009; 251:398–407. [PubMed: 19276322]

143. Zhang J, Tehrani YM, Wang L, et al. Renal masses: characterization with diffusion-weighted MR imaging--a preliminary experience. Radiology. 2008; 247:458–464. [PubMed: 18430878]

144. Kim S, Jain M, Harris AB, et al. T1 hyperintense renal lesions: characterization with diffusionweighted MR imaging versus contrast-enhanced MR imaging. Radiology. 2009; 251:796–807. [PubMed: 19380690]

145. Sandrasegaran K, Sundaram CP, Ramaswamy R, et al. Usefulness of diffusion-weighted imaging in the evaluation of renal masses. AJR Am J Roentgenol. 2010; 194:438–445. [PubMed: 20093607]

146. Wang H, Cheng L, Zhang X, et al. Renal cell carcinoma: diffusion-weighted MR imaging for subtype differentiation at 3.0 T. Radiology. 2010; 257:135–143. [PubMed: 20713607]

147. Rosenkrantz AB, Niver BE, Fitzgerald EF, et al. Utility of the apparent diffusion coefficient for distinguishing clear cell renal cell carcinoma of low and high nuclear grade. AJR Am J Roentgenol. 2010; 195:W344–W351. [PubMed: 20966299]

148. Chandarana H, Lee VS, Hecht E, et al. Comparison of biexponential and monoexponential model of diffusion weighted imaging in evaluation of renal lesions: preliminary experience. Investigative radiology. 2011; 46:285–291. [PubMed: 21102345]

149. Chandarana H, Kang SK, Wong S, et al. Diffusion-weighted intravoxel incoherent motion imaging of renal tumors with histopathologic correlation. Investigative radiology. 2012; 47:688–696. [PubMed: 22996315]

150. Bellomo R, Kellum JA, Ronco C. Acute kidney injury. Lancet. 2012; 380:756–766. [PubMed: 22617274]

151. Kellum JA, Bellomo R, Ronco C. The concept of acute kidney injury and the RIFLE criteria. Contributions to nephrology. 2007; 156:10–16. [PubMed: 17464110]

152. Palevsky PM. Chronic-on-acute kidney injury. Kidney international. 2012; 81:430–431. [PubMed: 22333743]

153. Coca SG, Cho KC, Hsu CY. Acute kidney injury in the elderly: predisposition to chronic kidney disease and vice versa. Nephron Clin Pract. 2011; 119(Suppl 1):c19–c24. [PubMed: 21832852]

154. He X, Aghayev A, Gumus S, et al. Estimation of single-kidney glomerular filtration rate without exogenous contrast agent. Magn Reson Med. 2013

155. Zimmer F, Zollner FG, Hoeger S, et al. Quantitative renal perfusion measurements in a rat model of acute kidney injury at 3T: testing inter- and intramethodical significance of ASL and DCE-MRI. PloS one. 2013; 8:e53849. [PubMed: 23308289]

156. Prowle JR, Molan MP, Hornsey E, et al. Measurement of renal blood flow by phase-contrast magnetic resonance imaging during septic acute kidney injury: a pilot investigation. Critical care medicine. 2012; 40:1768–1776. [PubMed: 22487999]

157. Singh P, Ricksten SE, Bragadottir G, et al. Renal oxygenation and haemodynamics in acute kidney injury and chronic kidney disease. Clinical and experimental pharmacology & physiology. 2013; 40:138–147. [PubMed: 23360244]

158. Rosen S, Epstein FH, Brezis M. Determinants of intrarenal oxygenation: factors in acute renal failure. Renal failure. 1992; 14:321–325. [PubMed: 1509164]

159. Li LP, Franklin T, Du H, et al. Intrarenal oxygenation by blood oxygenation level-dependent MRI in contrast nephropathy model: effect of the viscosity and dose. J Magn Reson Imaging. 2012; 36:1162–1167. [PubMed: 22826125]

160. Koff SA. Requirements for accurately diagnosing chronic partial upper urinary tract obstruction in children with hydronephrosis. Pediatr Radiol. 2008; 38(Suppl 1):S41–S48. [PubMed: 18074126]

161. Grattan-Smith JD, Perez-Bayfield MR, Jones RA, et al. MR imaging of kidneys: functional evaluation using F-15 perfusion imaging. Pediatr Radiol. 2003; 33:293–304. [PubMed: 12695861]

162. Vivier PH, Dolores M, Taylor M, et al. MR urography in children. Part 1: how we do the F0 technique. Pediatr Radiol. 2010; 40:732–738. [PubMed: 20182706]

163. Jones RA, Schmotzer B, Little SB, et al. MRU post-processing. Pediatr Radiol. 2008; 38(Suppl 1):S18–S27. [PubMed: 18071692]

164. Rohrschneider WK, Becker K, Hoffend J, et al. Combined static-dynamic MR urography for the simultaneous evaluation of morphology and function in urinary tract obstruction. II. Findings in experimentally induced ureteric stenosis. Pediatr Radiol. 2000; 30:523–532. [PubMed: 10993536]

165. Jones RA, Perez-Brayfield MR, Kirsch AJ, et al. Renal transit time with MR urography in children. Radiology. 2004; 233:41–50. [PubMed: 15317951]

166. Vivier PH, Blondiaux E, Dolores M, et al. Functional MR urography in children. J Radiol. 2009; 90:11–19. [PubMed: 19182709]
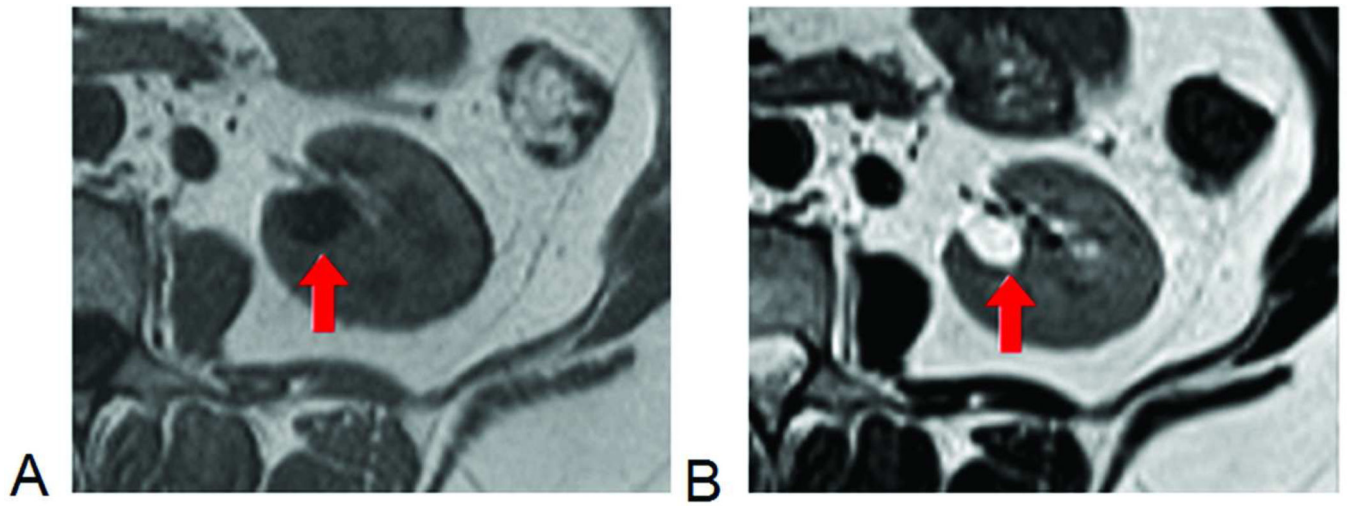
Figure 1.
Conventional anatomic MRI of kidney. The cyst, with long T_1, is dark on T_1-weighted image (A) and, with long T_2, bright on T_2-weighted image (B).
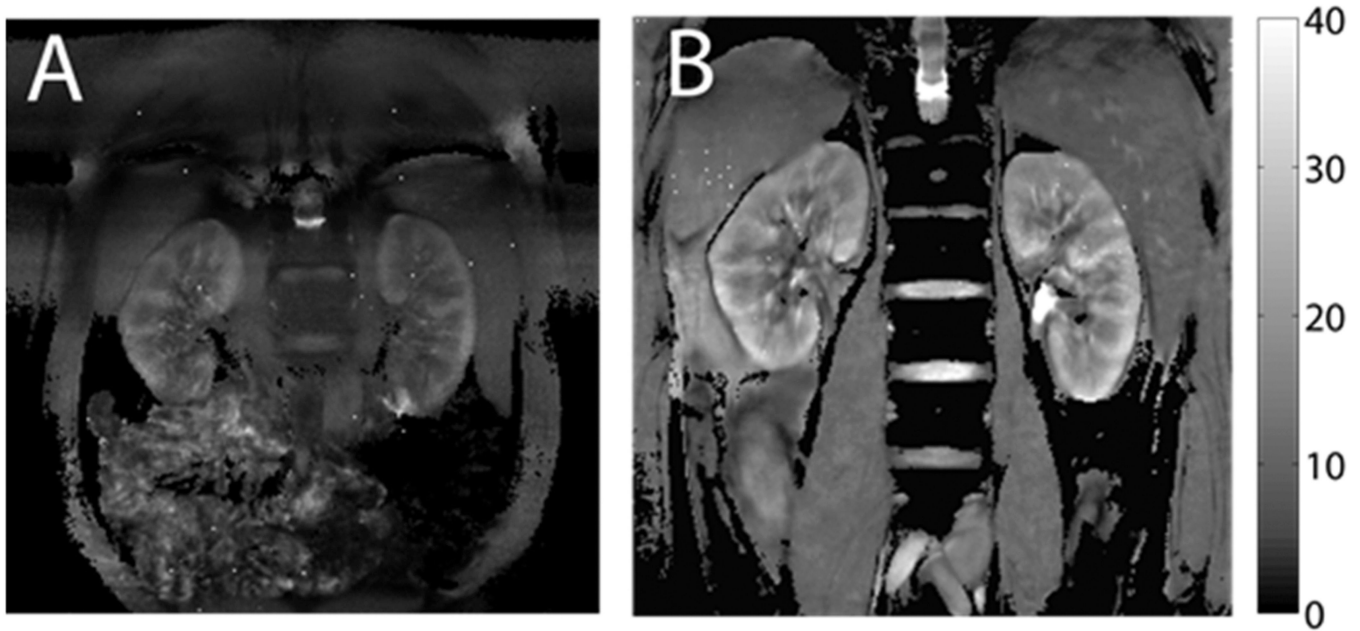
Figure 2.
Kidney T_2* maps from BOLD imaging. The scale on the right side is T_2* value, with unit of milliseconds. Higher T_2* corresponds to lower deoxyhemoglobin concentration. A) Typical T_2* map with conventional BOLD scan (20-sec breath-hold, matrix size 256×256, FOV 32×32 cm). B) T_2* map with free-breathing prospectively navigated sequence (10-minute imaging time, matrix size 512×512, FOV 50×50 cm). The free-breathing images offer greater image quality.
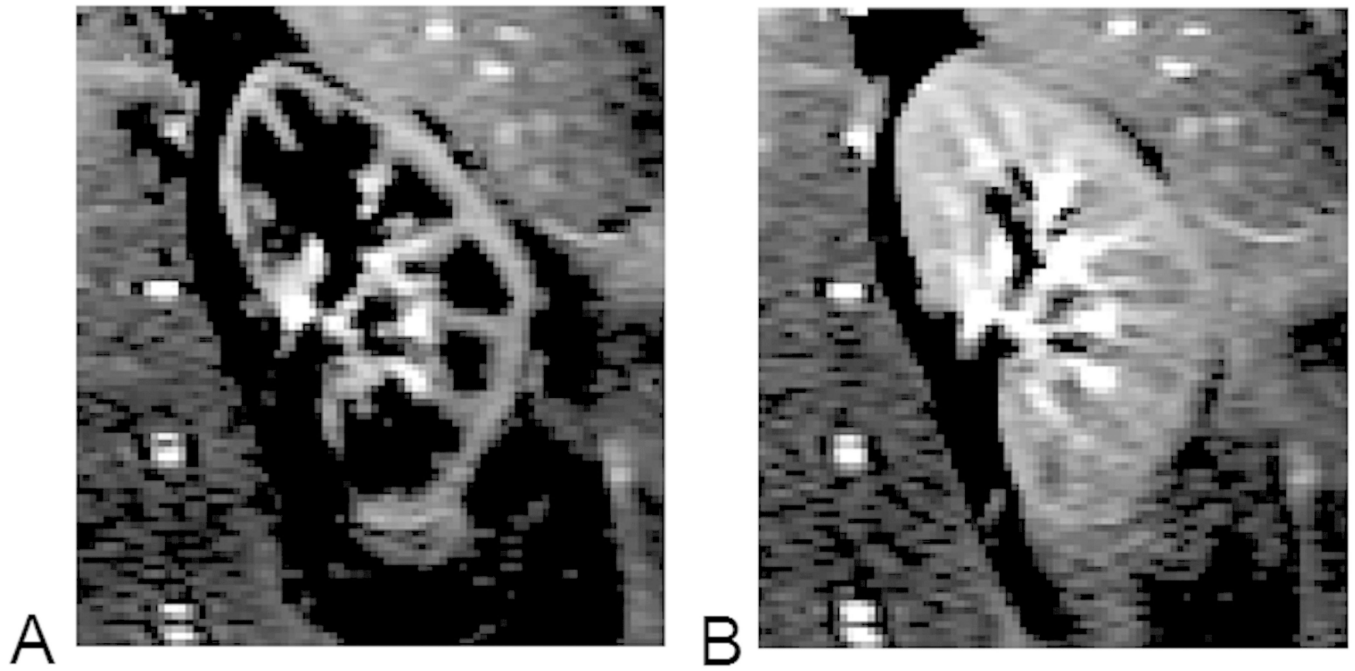
Figure 3.
Difference images obtained from renal ASL scans. A) Acquired at 800 ms after arterial blood labeling, when the labeled blood is mostly in renal cortex; B) 1000 ms after the labeling, and some labeled blood reaches renal medulla. The images were acquired by a modified TrueFISP FAIR ASL sequence (8 averages, acquisition time ~24 sec, with breath hold).

Figure 4.
Kidney diffusion-weighted imaging using DTI methods. Following imaging processing, color-coded primary diffusion eigenvectors display radial pattern of medullary tubules.
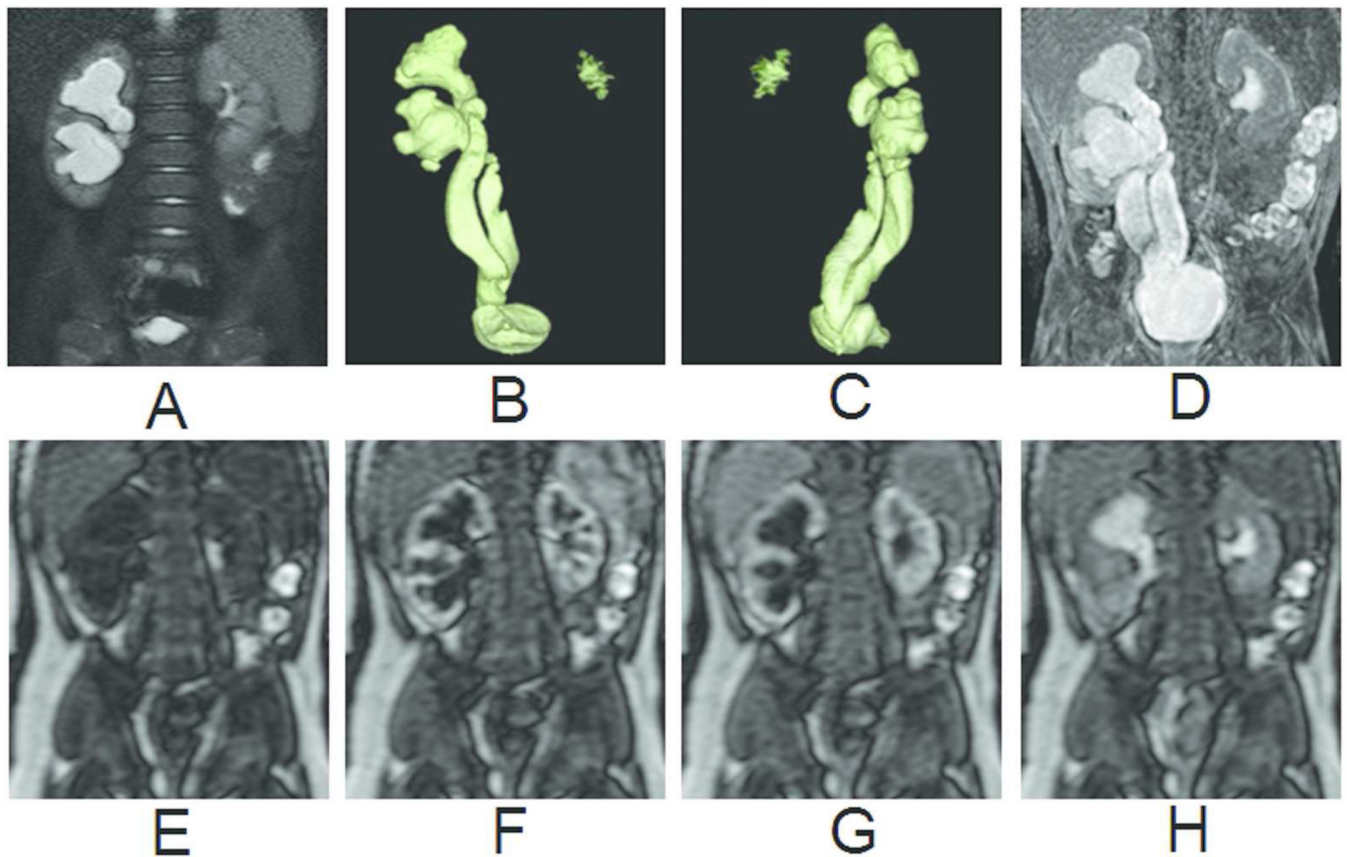
Figure 5.
Primitive right megaureter on a bifid ureter in a 6-month old boy. (A) T_2-weighted image with fat saturation. (B) Coronal view of volume-rendered T_2-weighted images. (C) Oblique view of volume-rendered T_2-weighted images. (D) Maximum intensity projection of T_1-weighted images at excretory phase. (E) Renography before contrast arrival. (F) Renography at arterial phase. (G) Renography at tubular phase. (H) Renography at excretory phase. Symmetric enhancement and excretion of contrast bilaterally suggests that the marked dilatation of the right collecting system and ureter is not a functional obstruction.

Table 1

A summary of major MRI techniques and their capabilities

Techniques	Capability	Parameters
Dynamic contrast enhanced MRI (DCE MRI)	Tracer transit through vascular space and tubules	GFR, perfusion, vascular and tubular mean transit times (MTT)
Blood oxygen level dependent (BOLD)	Direct measure of deoxyhemoglobin, and reflects blood and tissue pO_2	Spin-spin relaxation rate ($R_2^* = 1/T_2^*$), medulla-cortex R_2^* ratio (MCR $= R_2^*_{Med}/R_2^*_{Cx}$)
Arterial spin labeling (ASL)	Perfusion without injecting tracer	Perfusion
Diffusion weighted imaging (DWI)	Water diffusion in interstitial space; capillary flow	Apparent diffusion coefficient (ADC), anisotropy, perfusion fraction